Supplementary Figures

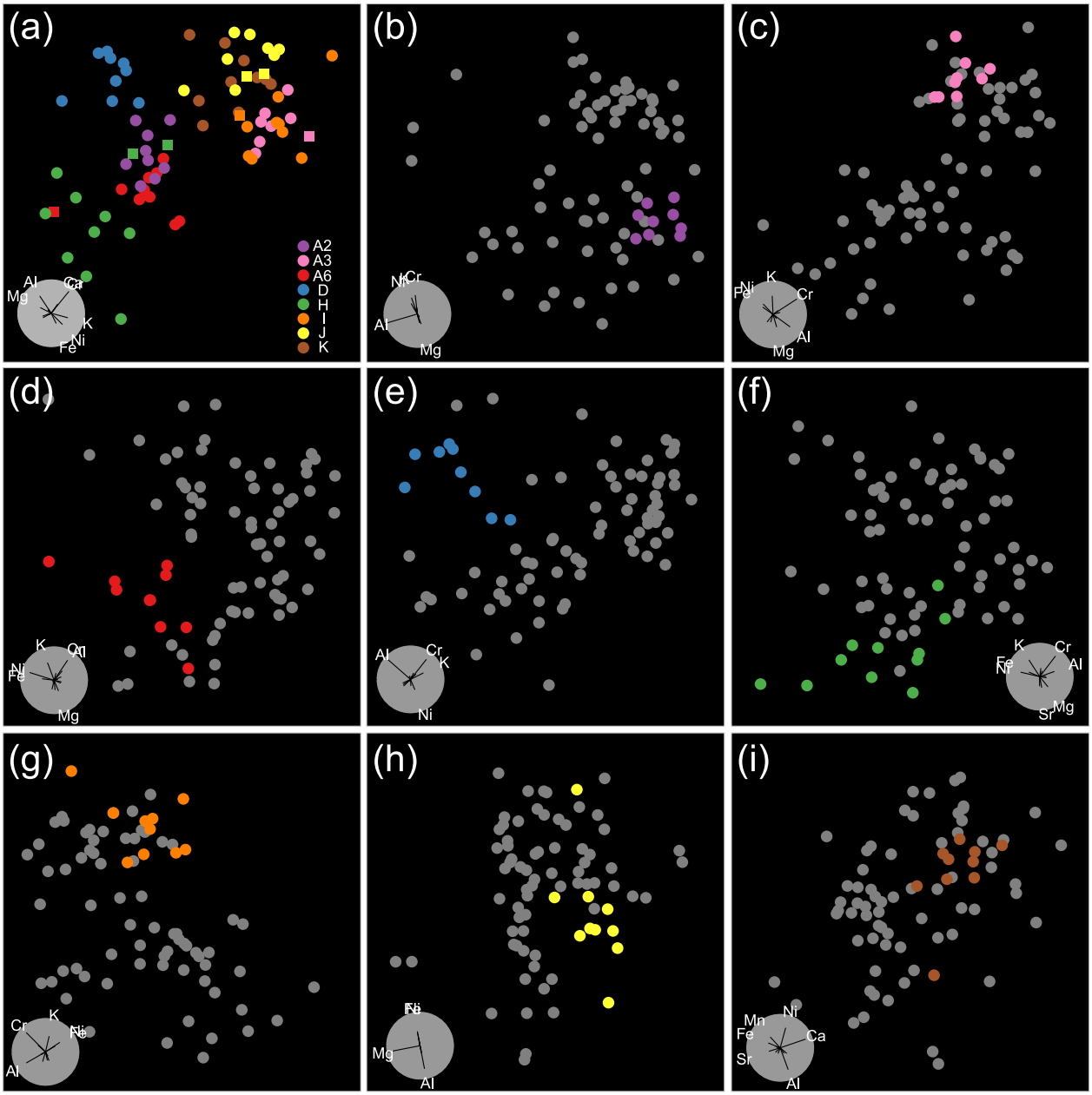

Supplementary Figure 1: YOY perch cluster into groups associated with the site from which they were captured based on a linear discriminant analysis (LDA) of total-body metal concentrations. Ten fish were sampled from each site A2, A3, A6, D, H, I, J, K and we measured concentrations of 15 elements using ICP-MS. The LDA successfully classified 90% of individuals into their respective sites using this multivariate dataset, though discrete separation of

groups was difficult to visualize in only two-dimensions. (a) Classification of fish into sites based on LDA along each axis of 15 elements (circles and squares show correct and incorrect classifications, respectively). Axis rotations shown in bottom-left hand corner. From this subplot, site A2 (purple) clusters together in a plane in front of site A6 (red) that connects between two points from site H (green). Site A3 (pink) similarly clusters in a plane behind site I (orange). Site A6 (red) clusters in a plane behind A2 (purple), except for one fish that was misclassified as site H. Site D (blue) is entirely distinct in this perspective, as are all but two fish in Site H (green), which were classified as A2 and A6. For site I (orange), fish cluster in a plane at the front of the plot, except for one that was in classified as A3 (pink). Although more difficult to visualize, site J (yellow) is in a separate plane in front of site K (brown), except for two points that were associated with K. Finally, all points in site K were separated in the far-back plane. (b–i) Points of each site are highlighted corresponding with the legend in (a). $n = 77$ for each panel as 3 fish could not be measured on the ICP-MS.

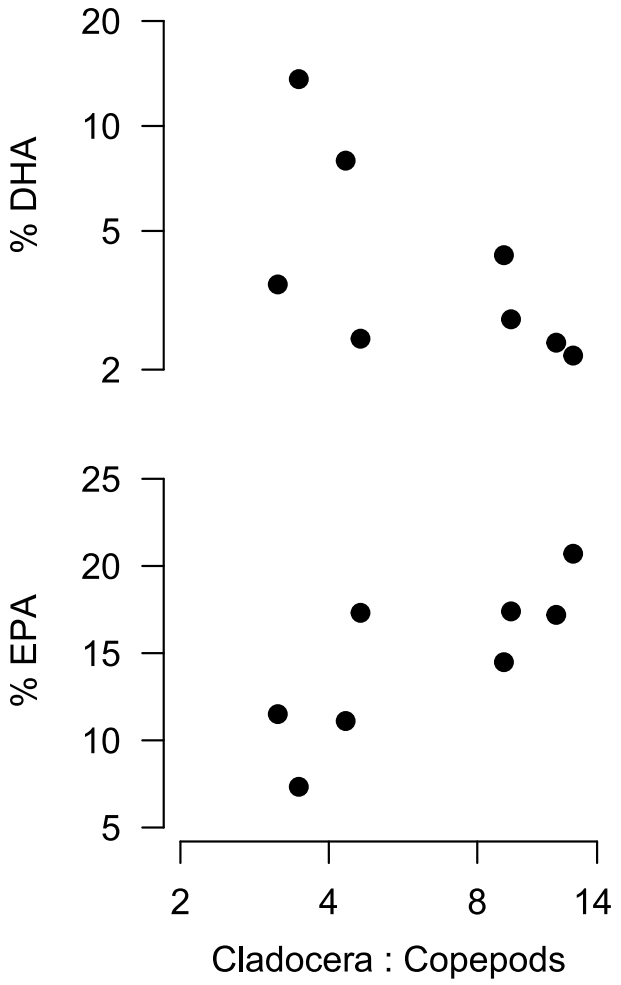

Supplementary Figure 2: Shifts in n-3 FA associated with increasing numbers of Cladocera relative to Copepoda in each site. (a) DHA and (b) EPA measured across days and sampling lines as percentage of total fatty acids in zooplankton communities. Zooplankton species were identified from horizontal tows conducted midday on July 3 and 4 with a 0.3 m wide, 1 m long conical plankton net (250 μm mesh). Tows were at a depth of 0.5 m for 10 m centered above each of three sampling lines running parallel to shoreline and each containing three vertically-deployed zooplankton traps positioned at a distance of at least 1 and 2 m from those on the same and adjacent sampling lines, respectively. Resulting samples contained 180 mL of lake water and were immediately preserved. We then counted all Copepoda and Cladocera zooplankton individuals and expressed a ratio for each site across all samples (n = 8).

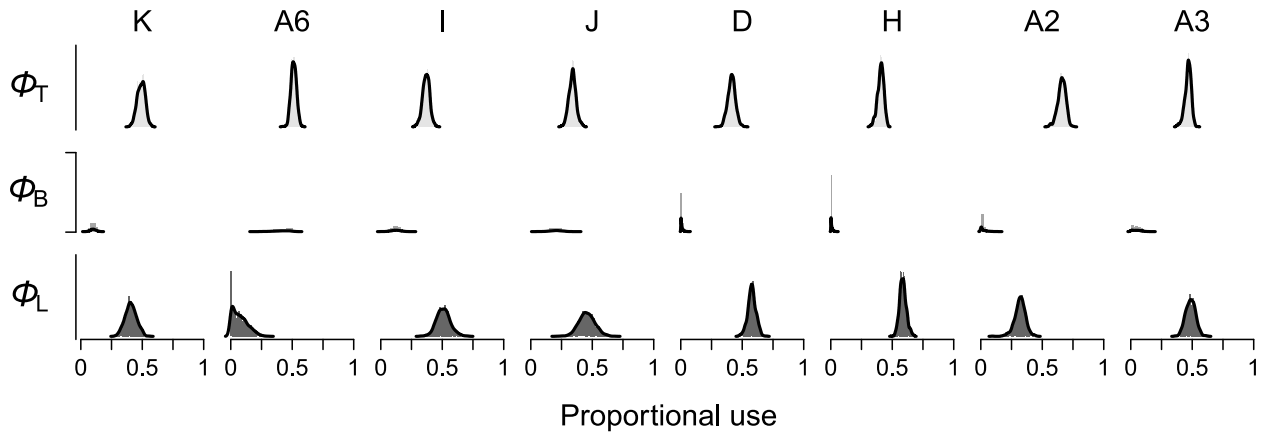

Supplementary Figure 3: Posterior probability estimates of resource use by YOY perch.

Use of terrestrial (ϕ_T), benthic (ϕ_B), and littoral (ϕ_L) resource was estimated separately at each of eight sites A2 – K. Solid lines are posterior probability density functions plotted upon histograms of posterior estimates. Sites are sorted in increasing mean NDVI within the entire sub-catchment.

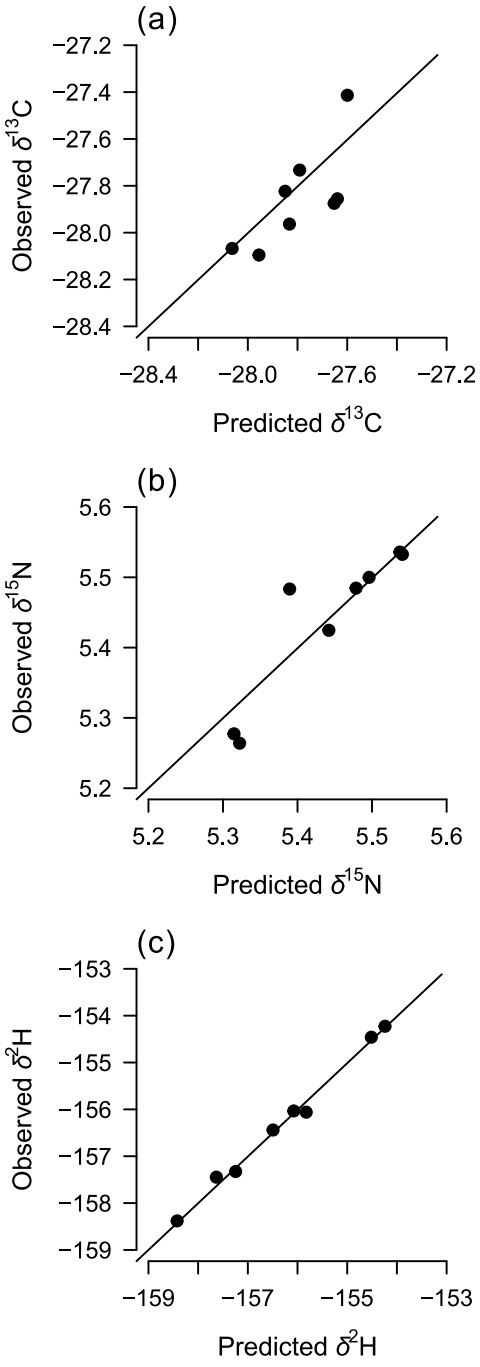

Supplementary Figure 4: Fit of three isotope mixing model. Predicted versus observed site-level ratios of (**a**) $\delta^{13}C$, (**b**) $\delta^{15}N$, and (**c**) $\delta^{2}H$. Points are average posterior estimates of site-level values and observed means in 15 YOY perch across each of 8 sites. Classical R^2 = 0.47, 0.81, and 0.99 when averaging posterior estimates (as plotted above). Bayesian R^2 = 0.45, 0.39, and 0.58, respectively, though values were highly conservative given the residual error.

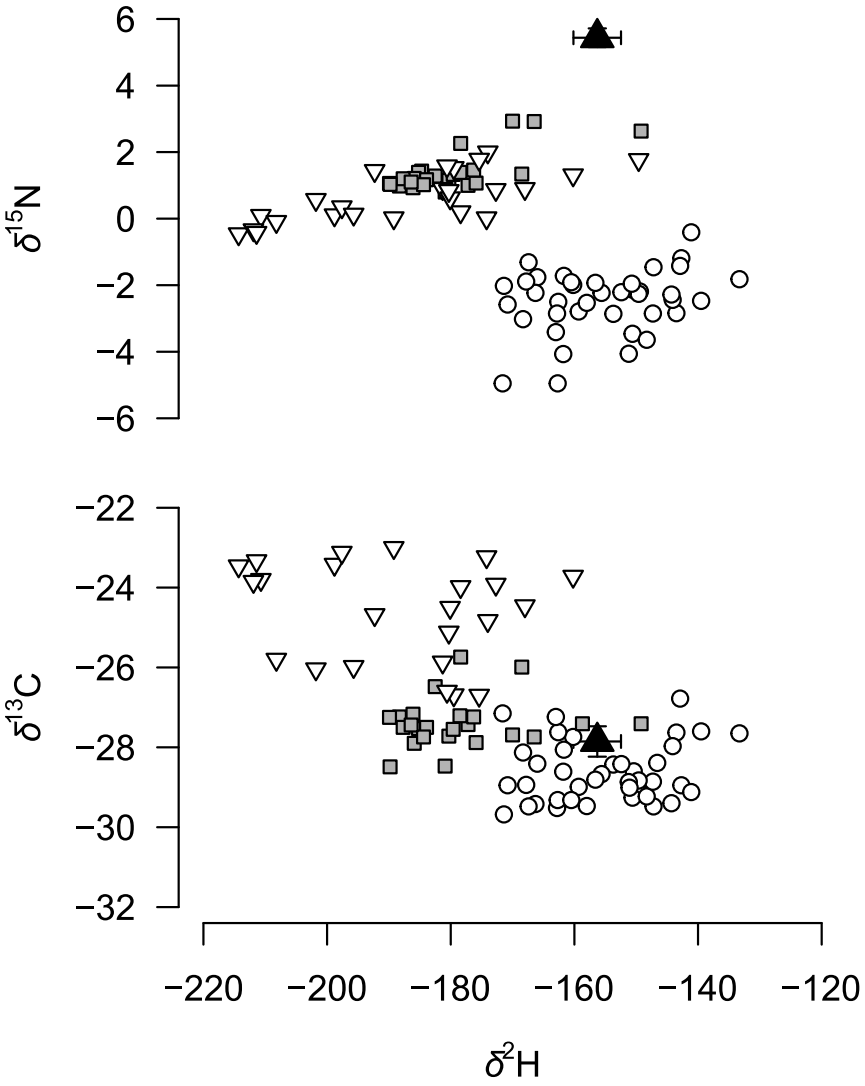

Supplementary Figure 5: Biplots of isotope data used in mixing models. The terrestrial, benthic, and littoral resources were respectively leaf litter (open circles; *n* = 40), periphyton (open inverted triangles; *n* = 24), and zooplankton (gray squares; *n* = 29 for $\delta^{13}C$ and $\delta^{15}N$; *n* = 40 for $\delta^{2}H$). Solid triangles show mean ± s.d. of stable isotope ratios for 120 YOY perch. Mean ± s.d. $\delta^{2}H$ for water was -66.4 ± 1.2 (*n* = 24).

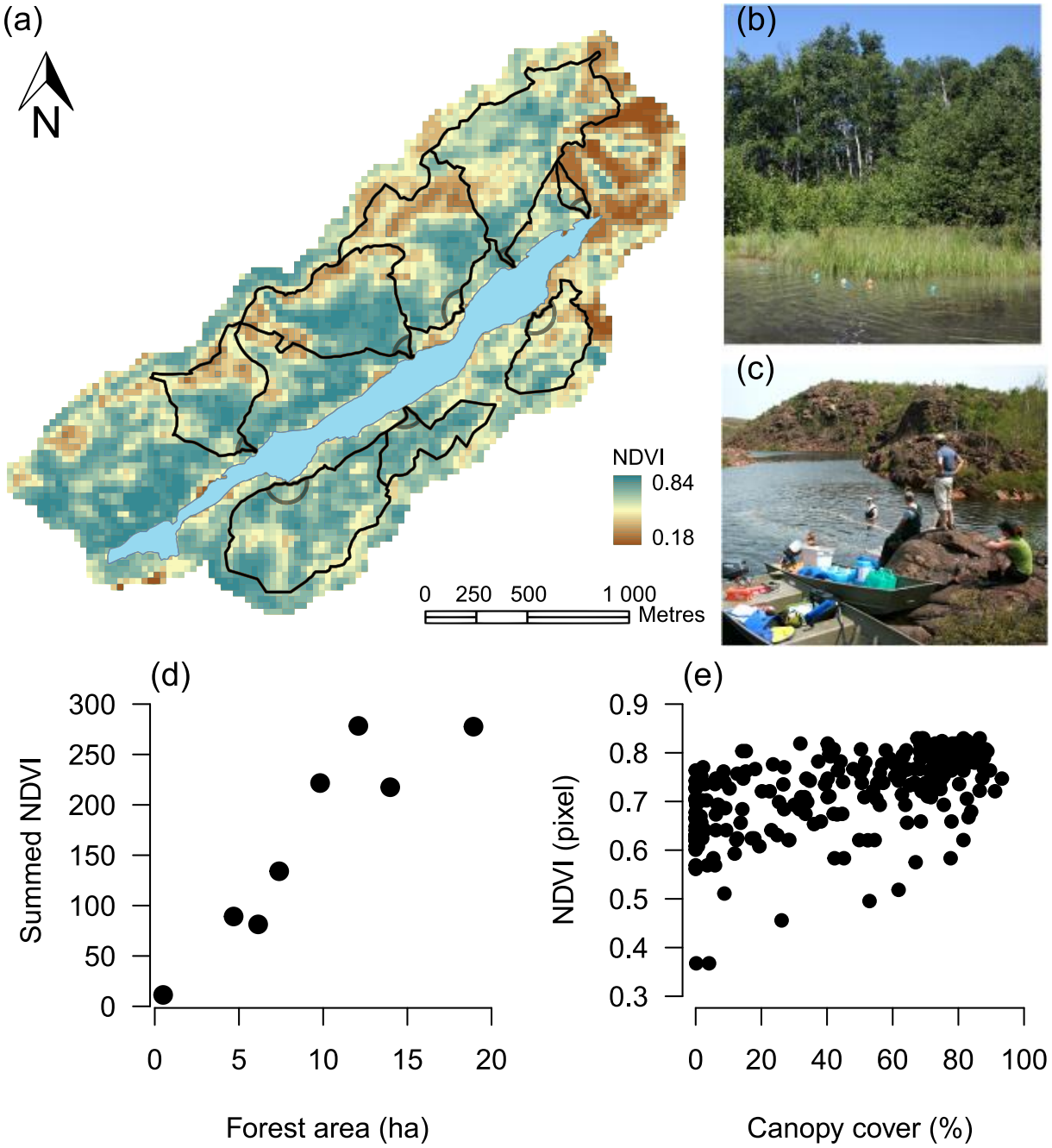

Supplementary Figure 6: Map of study catchments, showing vegetation density and NDVI. (a) NDVI (30 m × 30 m pixels) within boundaries of study catchments (black lines) and riparian zones 100 m from stream-lake interface (gray curves). Sites D, H, I, J, and K lie on the northern side of the lake in sequential order from the west to east, while A2, A3, and A6 occur on the southern side of the lake from west to east. (b) Site D (most westerly catchment on north side of

lake) in summer 2012, showing high vegetation density. (c) Site A6 (most easterly catchment on south side of lake) in summer 2012, showing low vegetation density surrounded by barren and exposed rock. (**d**) Absolute quantity of vegetation cover in each of 8 sub-catchments (summed NDVI) increases with forest area delineated from aerial photography. (e) NDVI in 30 m × 30 m pixels increases with nearest point estimate of canopy cover in nine sub-catchments (n = 23 – 30 random points per sub-catchment).

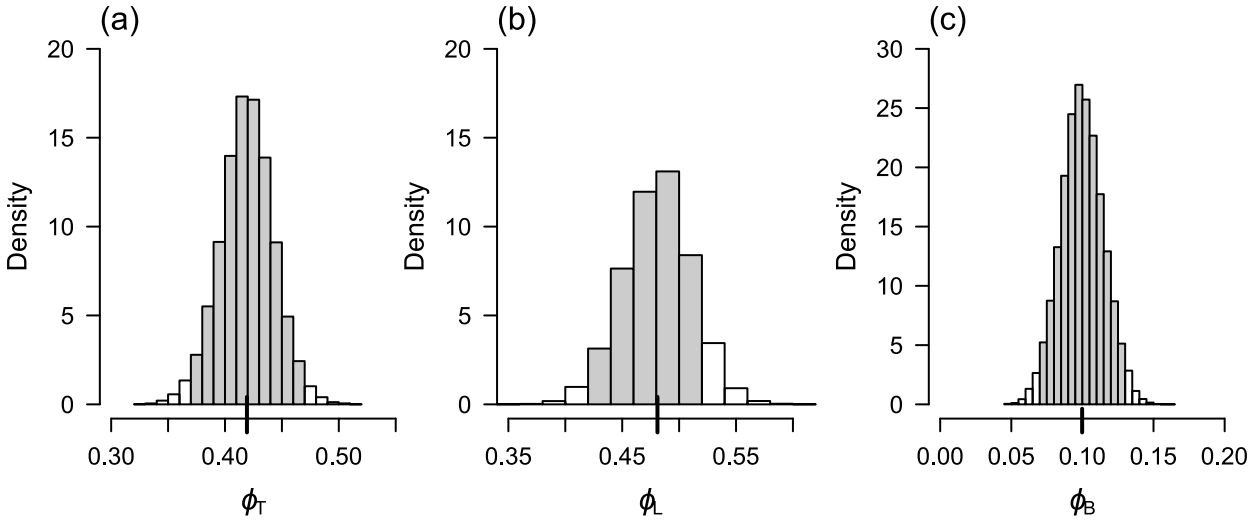

Supplementary Figure 7: Posterior probability densities of resource use estimated for simulated datasets of isotopic composition in YOY fish. Use of (**a**) terrestrial (ϕ_T), (**b**) littoral (ϕ_L), and (**c**) benthic (ϕ_B) resources estimated from a mixing model fitted separately to 99 simulated datasets. Mean of simulations denoted by vertical black line intersecting *x*-axis.

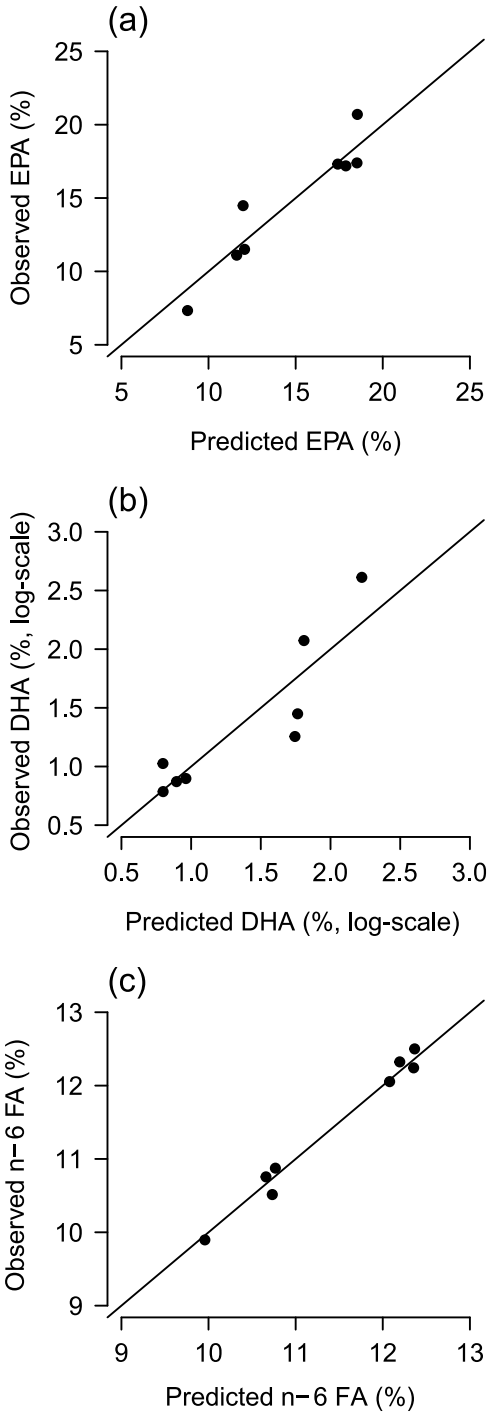

Supplementary Figure 8: Model fitted to predict fatty acids (FA) in zooplankton. (a) EPA, (b) DHA, and (c) n-6 FA content in zooplankton at each of 8 sites given values of unobserved latent variable representing overall FA composition available to fish [see Supplementary equation (8)]. Bayesian R^2 = 0.83, 0.71, and 0.95, respectively.

Supplementary Tables

Supplementary Table 1: **Mean mass fractions ± s.e.m. of eicosapentaenoic acid (EPA) and docosahexaenoic acid (DHA) in zooplankton species.**

Species	EPA	DHA	*n*
Diaphanosoma birgei	2.76 ± 0.23	3.04 ± 0.48	3
Holopedium gibberum	6.93 ± 2.05	1.04 ± 0.37	5
Epischura lacustris	5.12 ± 0.41	10.28 ± 1.33	5

Zooplankton were collected across five sites in Daisy Lake in 2010. Both *Diaphanosoma birgei* (Sididae) and *Holopedium gibberum* (Holopediidae) are Cladocera taxa, whilst *Epischura lacustris* (Temoridae) are Copepoda taxa. Values are reported in μg fatty acid methyl esters per mg of dry weight of tissue extracted.

Supplementary Table 2: Mean characteristics of YOY perch populations sampled in each site (± s.e.m.), sorted in in descending order for mean fish weight per site.

Site	Weight (g)	Age (days)	Growth rate κ_j †
I	0.491 (0.017)	54 (2)	0.43 (0.38 – 0.49)
H	0.434 (0.012)	N/A	0.37 (0.33 – 0.43)
J	0.409 (0.013)	N/A	0.35 (0.32 – 0.40)
D	0.379 (0.011)	N/A	0.33 (0.29 – 0.37)
A2	0.314 (0.011)	N/A	0.27 (0.23 – 0.31)
A3	0.303 (0.010)	N/A	0.25 (0.22 – 0.30)
K	0.299 (0.013)	N/A	0.25 (0.21 – 0.30)
A6	0.228 (0.008)	56 (2)	0.19 (0.15 – 0.23)

Weights were measured on 100 individuals per site, while age was estimated from 6 individuals only for sites I and A6 using saggital otoliths (see Supplementary Methods). Growth rates were estimated using the power function (Supplementary equation 13) allowing for growth period to vary among sites; 95% CI in parentheses. †Mean (95% CI) for other parameters in Supplementary equation (13): α_8 = 0.029 (0.001 – 0.062); θ = 0.016 (0.001 – 0.042); σ = 0.12 (0.12 – 0.13).

Supplementary Table 3: Estimated effects for models associated with trophic upsurge hypothesis and stable isotope analyses.

Parameter	Mean (95% CIs)
Supplementary equation (4) tPOC model (R^2 = 0.47)	
Intercept α_1	-1.54 (-2.23 – -0.84)
Effect of NDVI β_1	**0.72 (0.03 – 1.44)**
Effect of wetland cover β_2	**0.77 (0.01 – 1.51)**
s.d. in tPOC $\sigma^{(1)}$	0.86 (0.42 – 1.89)
Supplementary equation (5) DOC model (R^2 = 0.99)	
Intercept α_2	1.05 (1.04 – 1.07)
Effect of tPOC β_3	**0.02 (0.01 – 0.03)**
Effect of weighted wetland area β_4	**0.18 (0.17 – 0.20)**
s.d. in DOC $\sigma^{(2)}$	0.02 (0.01 – 0.04)
Supplementary equation (6) Bacteria model (R^2 = 0.95)	
Intercept α_3	5.76 (5.45 – 6.04)
Effect of DOC β_5	**0.06 (0.02 – 0.14)**
Effect of fluoresence index β_6	**0.06 (0.02 – 0.11)**
Effect of thirty-nine replicates β_7	**-0.37 (-0.47 – -0.29)**
Effect of water temperature β_8	-0.02 (-0.06 – 0.01)
Effect of phytoplankton abundance β_9	**-0.05 (-0.11 – -0.02)**
s.d. among dates $\sigma_{\varepsilon j}$	0.18 (0.08 – 0.94)
s.d. among sites $\sigma_{\varepsilon i}$	0.03 (0.01 – 0.08)
Supplementary equation (7) Zooplankton model (R^2 = 0.50, classical R^2 = 0.96)	

Intercept α_4	2.02 (1.56 – 2.36)
Effect of bacterial densities β_{10}	**0.69 (0.10 – 1.32)**
Effect of tPOC quantity β_{11}	-0.48 (-1.96 – 0.15)
Effect of tPOC quality β_{11}	-0.26 (-0.80 – 0.22)
Effect of high-quality phytoplankton densities β_{13}	0.26 (-0.26 – 0.63)
Effect of predation pressure β_{14}	**-0.96 (-1.72 – -0.20)**
s.d. in zooplankton $\sigma^{(3)}$	0.43 (0.14 – 1.41)

Supplementary equation (8) Fish size model 1 (R^2 = 0.98)

Intercept at low predation α_5	-1.07 (-1.13 – -0.92)
Change in intercept with high predation α_6	-0.07 (-0.36 – 0.02)
Effect of zooplankton β_{15}	**0.25 (0.07 – 0.49)**
Effect of water temperature β_{16}	0.02 (-0.27 – 0.18)
Effect of perch density β_{17}	-0.04 (-0.14 – 0.07)
Effect of overall fatty acids β_{18}	**0.23 (0.14 – 0.49)**
Effect of overall fatty acids on EPA γ	**0.88 (0.42 – 1.67)**
Effect of overall fatty acids on DHA γ	**-0.85 (-1.71 – -0.36)**
Effect of overall fatty acids on n-6 FA γ	**0.94 (0.52 – 1.78)**
s.d. in fish $\sigma_i^{(4)}$	0.33 (0.26 – 0.43)
s.d. in fatty acids independent of zooplankton $\sigma^{(5)}$	0.72 (0.37 – 1.63)
s.d. in EPA	0.42 (0.22 – 0.95)
s.d. in DHA	0.53 (0.33 – 1.14)
s.d. in n-6 FA	0.21 (0.03 – 0.69)

Supplementary equations (9–10) Three-isotope mixing model

$\phi_{T,1}$	0.66 (0.59 – 0.71)
$\phi_{T,2}$	0.47 (0.41 – 0.51)
$\phi_{T,3}$	0.51 (0.47 – 0.56)
$\phi_{T,4}$	0.41 (0.35 – 0.47)
$\phi_{T,5}$	0.41 (0.35 – 0.45)
$\phi_{T,6}$	0.37 (0.31 – 0.42)
$\phi_{T,7}$	0.34 (0.28 – 0.40)
$\phi_{T,8}$	0.49 (0.43 – 0.55)
$\phi_{L,1}$	0.32 (0.22 – 0.40)
$\phi_{L,2}$	0.49 (0.41 – 0.56)
$\phi_{L,3}$	0.06 (<0.01 – 0.21)
$\phi_{L,4}$	0.58 (0.51 – 0.64)
$\phi_{L,5}$	0.59 (0.54 – 0.65)
$\phi_{L,6}$	0.51 (0.40 – 0.63)
$\phi_{L,7}$	0.45 (0.33 – 0.59)
$\phi_{L,8}$	0.41 (0.32 – 0.50)
$\phi_{B,1}$	0.01 (<0.01 – 0.09)
$\phi_{B,2}$	0.05 (<0.01 – 0.12)
$\phi_{B,3}$	0.42 (0.27 – 0.51)
$\phi_{B,4}$	<0.01 (<0.01 – 0.04)
$\phi_{B,5}$	<0.01 (<0.01 – 0.03)
$\phi_{B,6}$	0.12 (0.04 – 0.19)
$\phi_{B,7}$	0.21 (0.10 – 0.30)

$\phi_{B,8}$	0.10 (0.06 – 0.14)
Δ_N	2.34 (0.32 – 4.46)
Δ_{tot}	5.86 (5.63 – 6.02)
τ	2.48 (2.28 – 2.70)
ω_{tot}	0.06 (<0.01 – 0.17)
s.d. among sites σ_ϕ	0.10 (<0.01 – 0.54)
Residual s.d. in $\delta^{13}C$ σ_C	0.01 (<0.01 – 0.04)
Residual s.d. in $\delta^{15}N$ σ_N	0.02 (<0.01 – 0.05)
Residual s.d. in $\delta^{2}H$ σ_H	8.67 (5.34 – 12.9)
Degrees of freedom in Student-*t* distribution ψ	6.65 (3.28 – 23.4)

Supplementary equation (11) Change in ϕ_T with catchment land cover (logit scale)

Mean terrestrial support across sites α_T	-0.22 (-0.46 – <-0.01)
Effect of NDVI $\beta_{T,1}$	**0.34 (0.15 – 0.58)**
Effect of catchment size $\beta_{T,2}$	**-0.28 (-0.53 – -0.12)**
Effect of wetland area $\beta_{T,3}$	**0.27 (0.11 – 0.42)**
Interaction of NDVI and wetland area $\beta_{T,4}$	**0.45 (0.26 – 0.69)**

All covariates described in Supplementary Methods and were standardized to a mean of zero and s.d. of one in regressions so that effects are directly comparable. Bolded effects (β, γ) do not overlap zero. We report a Bayesian R^2 as a measure of model fit (83). For the zooplankton model (Supplementary equation 7), R^2 was highly conservative because of relatively large residual error; classical R^2 was 0.96 when averaging posterior estimates of site-level abundance.

Supplementary Table 4. Estimated effects in final models predicting Ba:Ca and Sr:Ca in 9-10 perch from each of 8 sites [see Supplementary equation (13)].

	Ba:Ca		Sr:Ca	
Effect	Mean	95% CIs	Mean	95% CIs
Water molar ratio (β_{22})	**0.07**	**0.03 – 0.10**	**0.05**	**0.03 – 0.06**
Fish mass (β_{23})	**-0.14**	**-0.18 – -0.10**	**-0.07**	**-0.09 – -0.05**
Wetland area (β_{24})	0.03	-0.01 – 0.07	0.03	0.01 – 0.04
Intercept (α_9)	-0.91	-0.94 – -0.87	1.63	1.61 – 1.64
Residual error (σ)	0.16	0.14 – 0.19	0.07	0.06 – 0.09

Model predictors were water molar ratio (mmol mol^{-1}), fish mass (g), and weighted wetland area (ha). All effects were standardized to a mean of zero and s.d. of one, so are directly comparable. Bolded effects do not overlap zero. Bayesian R^2 = 0.44 and 0.54 for the Ba and Sr models, respectively.

Supplementary Notes

Supplementary Note 1: Alternative models explaining variation in biomass stocks

Trophic cascades

There was weak evidence for trophic cascades that might explain the accumulation of biomass at different levels of the food web. Specifically, we tested whether biomass stocks of lower food web components were regulated by upper-level components. Under a model of trophic cascades, we expected that the absence of top-predators in some sites promoted: (i) a high biomass stocks of YOY perch, which (ii) reduced biomass of zooplankton, and subsequently (iii) increased bacterial densities.

Our statistical models already tested conditions (i) and (ii) of the trophic cascade hypothesis (Supplementary Table 3). For YOY fish, we found that their biomass did not increase as fewer top predators were caught in each site (95% CI for effect: -0.02 – 0.36), although our sampling was relatively limited. Similarly, trophic cascades were not the dominant force structuring zooplankton communities when we considered condition (ii). Predation pressure upon zooplankton by planktivorous fish was certainly important in reducing biomass trapped at each site (95% CI: -1.72 – -0.20), but this effect overlapped with the bottom-up effect that increased bacterial densities (95% CI: 0.10 – 1.32). Finally, we could not include zooplankton abundance in our model of bacteria densities because parameter estimates for the associated effect were correlated with water temperatures (r >0.80). Replacing water temperatures in Supplementary equation (6) with the total amount of zooplankton biomass caught at each site, however, did not improve model fit or reduce bacterial densities (95% CI for effect -0.03 – 0.07, model R^2 = 0.89). The positive effect of DOC concentrations was unchanged (95% CI 0.02 –

0.13). Our findings are consistent with nearby lakes where there is little evidence that zooplankton can control phytoplankton biomass (1).

Variable hatching date:

Weights of YOY perch did not vary among sites simply because of site-specific differences in hatching dates. Our data supported this claim in two ways.

Otoliths: Microanalysis of otoliths revealed that fish were not larger simply because they were older. Six fish were randomly selected from the sites where we recorded the largest and smallest YOY weights. One sagittal otolith from each of the twelve YOY was then prepared under a compound microscope following standard methods for age determination (2). Using the hatch check as a reference point, daily increments between the hatch check and edge were counted 2–4 times along as many growth axes as possible (2). The most reliable and/or mean increment count was recorded as total age by a trained observer (S. Campana, Otolith Technologis, Stillwater Lake, NS). We did not inform the observer of the sites from which fish were selected so as to eliminate any possible bias.

Fish differed in size but not age between sites based on two-sample *t*-tests comparing mean values. The mean weight ± s.e.m. of the six YOY in site I was 0.45 ± 0.03 g versus 0.26 ± 0.03 g in site A6 (t_{10} = -4.43, p = 0.001). However, the mean age of YOY of did not differ between sites I and A6, with means ± standard errors of 54 ± 2 days and 56 ± 2 days, respectively (t_{10} = 0.59, p = 0.571).

Our findings are supported from many observational studies on the life history of larval perch. First, hatching and spawning usually occurs within a tight window of one to two weeks within a region (3–6). However, aging of otoliths suggests that such differences are absent within the small lake that we study. This likely arises because YOY fish all originate from a

common stock. Specifically, spawning typically occurs at a few sites, where the rate of egg development and timing of hatching are likely to be very similar (7). These larval populations then group almost immediately into the pelagic zone, where they continue development for approximately a fortnight, until randomly dispersing across a broad range of littoral sites (7). Heterogeneity in the littoral sites drives ensuing variation in fish size and fish spent sufficiently long in these sites between hatching and capture to differ in their trace metal signatures (Supplementary Fig. 1). Finally, local water temperatures exert critical controls over rates of egg development and timing of hatching (3, 8), but these did not vary across our sites during the first week of spring measurements (May 23–29), as determined by overlapping 95% CIs in a model predicting mean daily water temperatures at each site.

Growth modelling: Mean growth rates of fish estimated at each site from our data still differed when we allowed hatching dates, and hence growth period, to vary. We demonstrated this by separately fitting three of the most widely-used fisheries growth models to the YOY weight data: the von Bertalanffy growth model (VBGM), the Gompertz curve, and a simple power model that does not assume asymptotic growth like the former two approaches (9–12). The VBGM is a simplification of mechanistic bioenergetics models that can be estimated statistically (13, 14) and has been shown to fit the growth of yellow perch in Ontario lakes better than alternative models (15). Broadly, the VGBM predicts that growth rate (i.e. change in mass over time) arises from the difference between energy assimilation and loss, which are a function of weight W_t at time t (13). The integrated form of this function can then be used to predict the mean growth of each individual fish i at site j between time = 0 (and $W = 0$) to time = t as:

$$W_{ijt} = W_{\infty}[1 - e^{-k_j t(1-d)}]^{1/(1-d)}, \quad (1)$$

where W_{∞} is the estimated upper asymptote of body mass for a YOY perch, k_j is an estimated rate parameter for energy loss that determines growth differences among sites, and d is an estimated

parameter that scales consumption with body size and is likely to be relatively invariant among sites because it captures fundamental metabolic processes governing biomass production and maintenance across taxa (e.g. 14). The Gompertz model is similar to the VGBM but typically differs in estimates of its upper asymptote (9) and takes the form:

$$W_{ijt} = W_{\infty}e^{-ge^{-r_j t}}, \quad (2)$$

where e^{-g} is the estimated proportion of growth achieved at $t = 0$, which should be identical among sites given that individuals are likely derived from a common pool of eggs before colonizing different sites (see above), and r_j is an estimated rate of exponential decline in growth with age. Finally, the power function assumes that growth increases exponentially over time given an estimated scaling coefficient κ_j and exponent θ and estimated size α_8 at $t = 0$:

$$W_{ijt} = \alpha_8 + \kappa_j t^{\theta}. \quad (3)$$

We then tested whether we could eliminate differences in growth rates among sites, i.e. overlapping parameter estimates, by introducing variation into hatching dates. We did so by first assuming that perch grew for 60 days prior to measurement, because they hatched on May 7 2012. Field data from our study site do indicate that perch spawn in April shortly before our assumed hatch date (16), and eggs have been shown elsewhere to hatch in ca. 15 – 25 days (3–6). We then allowed for large variation in hatching period by scaling values between 30 and 90 based on average fish size in each site. Thus, sites with the largest fish were assumed to have grown the longest (90 days) and sites with the smallest fish were assumed to have grown the least 30 days). As discussed above in relation otoliths, evidence points to a tight window of hatching and spawning within regions, which never exceed the 60 day difference in the same lake we have used in our analyses (3–6). The exactness of the hatching date is also irrelevant for our aims

because we test whether relative rather than absolute variation among sites in hatching dates can explain observed differences in growth.

We fitted each model described by Supplementary equations (1–3) separately using MCMC sampling described in Supplementary Methods. We assumed fish weights were drawn from normal distributions with site-level means equal to Supplementary equations (1–3) and estimated standard deviations. All regression coefficients were given uninformative priors and we calculated 95% CIs from a subset of simulations once MCMC chains converged. We then compared support among models using log-likelihoods, with higher values being more strongly supported. There was no need for information criterion that penalize model fit based on number of parameters because each model had the same number of estimated parameters. Importantly, our aim was not to model individual growth rates but simply to estimate mean site-level parameters and test whether they differed among sites, as measured by non-overlapping 95% CIs.

We found that the power function was the most strongly supported model as it had the highest log-likelihood by >2, on average, compared with the VBGM, which was the next most supported model. The model predicted that the growth parameter κ_j in Supplementary equation (3) varied from 0.38 – 0.49 (95% CI), where fish were hatched the longest and were also the largest in size, to 0.15 – 0.23 (95% CI) in the site where fish had been hatched for the shortest period. This clearly shows that fish were larger because of their growth rates not growth periods (Supplementary Table 2).

Supplementary Methods

Estimating quantity of terrestrial biomass

We estimated terrestrial biomass in each site from satellite imagery. We obtained eleven Landsat 5 TM images from March 27 to October 5, 2011 that were free of cloud cover. The normalized difference vegetation index (NDVI) was calculated within 30 m × 30 m pixels for each image after determining "top of atmosphere" reflectance values, which allow NDVI comparison among images (17). NDVI is proportional to the absorption of photosynthetically active radiation, and so is an indicator of vegetation density (18). Values approaching 1 indicate high vegetation density, such as in closed-canopy forest, while values approaching -1 indicate barren land with little plant cover. We worked with 2011 images because organic matter produced and accumulated during this year, such as litterfall, will be washed into the streams that drain each site the following spring, and so best capture terrestrial subsidies to aquatic food webs in 2012. The presence of striping patterns due to a failure of the Scan Line Corrector aboard the Landsat 7 satellite in 2003 also prevented complete interpretation of composite 2012 Landsat 7 images, but this was not an issue with Landsat 5, which terminated routine acquisitions after 2011.

For each site, we derived a measure of riparian vegetation density for use in our analyses. We combined the multiple Landsat images using maximum value compositing (19), which only retains the maximum NDVI value recorded in each pixel among the eleven images. This has the advantage of minimizing atmospheric properties, such as clouds and water vapor, which reduce NDVI estimates (20). We then averaged NDVI values across all pixels within 100 m of each lake-stream interface (Supplementary Fig. 6a). All spatial data manipulation and analyses were conducted using ArcGIS 9.3 (ESRI, Redlands, CA).

Landsat estimates correlated closely with three independent measures of vegetation cover. First, NDVI estimates from Landsat summed within each site increased with NDVI calculated from high-resolution (0.4-m) images (r >0.98 at 0.4–30.0 m resolutions), which were obtained in 2007 using a Leica ADS40 Airborne Sensor (21). The Landsat estimates also increased with forest area (r = 0.92; Supplementary Fig. 6d), delineated from a 1:40 000 m aerial photograph taken in 2003 (22). Finally, NDVI estimates from Landsat increased with canopy cover (Spearman's rank correlation, $\rho = 0.61$, $p < 0.001$, $n = 260$; Supplementary Fig. 6e), measured in 2008 using a spherical densitometer at between 23 to 30 random sampling points within 100 m of the lake-stream interface in nine sub-catchments (22), seven of which we study here.

Quality of organic OM at different trophic levels

POC and DOC: POC quality was calculated as the ratio of total organic to total inorganic matter trapped across the eight sediment tubes at a site. Inorganic matter was simply the amount of mass that was not lost during combustion of organic material (see main text).

We also estimated DOC quality for each water sample using absorbance and fluorescence spectroscopy. Absorbance scans were taken across a wavelength range of 220 – 600 nm with a Varian Cary 60 UV-Vis spectrophotometer (Agilent Technologies, Santa Clara, CA). Three-dimensional fluorescence scans were performed by measuring emissions from 300 – 600 nm in 2 nm steps at 5 nm increments in excitation from 220 – 450 nm using a Cary Eclipse fluorescence spectrophotometer (Agilent Technologies, Santa Clara, CA). The resultant fluorescence excitation-emission matrices were instrument corrected, and adjusted for inner filter effects using sample absorbance scans. We then compared differences in DOC structure among sites by calculating the fluorescence index (FI) as the ratio of emission intensity observed at 470 nm divided by the intensity observed at 520 nm, both at an excitation of 370 nm (23). FI is a widely-

used index of fluorescence and absorbance properties (24), whereby increasing values suggest less aromaticity and a smaller degree of conjugation (23).

Zooplankton: We estimated the quality of zooplankton available to fish in each site from their composition of fatty acids (FA). Animals cannot entirely synthesise n-3 and n-6 FA because they lack the desaturase enzymes required for inserting a double bond into the n-3 or n-6 position (from the methyl end) of n-9 chains (25). Further, the ability of most animals to elongate and desaturate 18 carbon polyunsaturated FA to 20 or 22 carbon long chain polyunsaturated FA (LC-PUFA) is often inadequate (26). Thus, the growth, survival, and fitness of zooplankton and fish depends on obtaining LC-PUFA, such as eicosapentaenoic acid (EPA; 20:5n-3) and docosahexaenoic acid (DHA, 22:6n-3), from their diets (27, 28).

We measured the FA composition of zooplankton samples as methyl esters on a gas chromatograph following methods outlined in McMeans et al. (29). Fatty acid methyl esters were quantified from the total lipid extract using a Supelco SP-2560 column (Sigma-Aldrich Corp., St. Louis, MO) on a Hewlett Packard 6890 gas chromatograph (splitless injection), and then identified using a 37-component standard (Supelco 47885-U).

There is still uncertainty as to the specific FA required by fish and how these might vary with age and species (30), so we defined high-quality forage in terms of a high relative abundance of EPA, DHA, and n-6 FA. EPA and DHA account for between 68 – 78% of all n-3 FA measured within each site, while no specific n-6 FA were similarly dominant. Smith et al. (31) found that silver perch (*Bidyanus bidyanus*) grew faster when their diets were supplemented with the n-6 linoleic acid (LNA; 18:2n-6), and Brown et al. (32) speculated that LNA was critical for the development of yellow perch (*Perca flavescens*). Other n-6 fatty acids, such as arachidonic acid (20:4n-6), have been shown to promote the growth of marine species, such as juvenile turbot (*Scophthalmus maximus*) (33), and are rapidly accumulated upwards through

freshwater food webs (34). Similarly, the n-3 FA EPA and DHA are also nutritionally important for fish (30, 34), and were found to be the most abundant n-3 FA in a study of YOY perch (35), including within 24 YOY collected from five sites at Daisy Lake in 2010. EPA itself promotes development and growth, and maintains immunity to disease and pathogens (36–38).

Measures of habitat quality

Water temperature: Temperature affects the growth of bacteria (39–41), zooplankton (42), and YOY perch (e.g. 43, 44). Thus, we anchored three StowAway TidbiT water temperature loggers (Onset Computer Corp., Bourne, MA) in each site prior to any biotic sampling, and included the average of water temperatures recorded every 15 minutes from May 23 to June 24 2012 in our statistical analyses.

Fish predation pressure: We measured relative differences in predation on zooplankton communities and YOY perch by sampling the entire fish community at each site on July 12 and 13 using standardized multimesh gill nets (45). This method uses benthic monofilament gillnet gangs composed of 12 panels (each 2.5 m long × 1.2 m deep) of geometrically increasing mesh sizes (10–110 mm), in order to capture fish without any size dependence. We set nets outwards perpendicular from the shoreline starting at a depth of 1.0 m in order to capture fish activity within our focal study areas. The nets were deployed between 18:00 and 20:00 hours and were retrieved the next morning between 08:00 and 10:00 hours, after which they were immediately processed. We identified and counted each individual and measured total body length. The resulting number of individuals caught for each species is ultimately proportional to the species' population size and so measures relative abundance (45).

Statistical analysis of trophic upsurge hypothesis

POC: We tested if POC captured beneath each site increased with riparian vegetation. We summed the quantity of POC captured among the eight sediment traps at each site to derive a total POC (tPOC; g) value. POC ranges from 1.5-250 μm in size so should capture transfer of terrestrial OM into DOC (<1.5 μm). We assumed that $tPOC_i$ in each site *i* followed a log-normal distribution and varied with the quantity and quality of OM exported from land, respectively measured by the density of riparian vegetation within 100 m of the lake-stream interface ($NDVI_i$) and the percent of the catchment area covered by wetland (W_i, square-root transformed), which was measured from 1:40 000 aerial photographs taken in 2003 (22):

$$tPOC_i \sim \ln N(\mu_i^{(1)}, \sigma^{(1)}),$$

$$\mu_i^{(1)} = \alpha_1 + \beta_1 NDVI_i + \beta_2 W_i, \quad (4)$$

where α_1 is the mean estimated tPOC across sites and $\sigma^{(1)}$ is the estimated standard deviation (s.d.). Biogeochemical processes within wetlands influence nutrient ratios and particle sizes of POC exported from land (46), so their relative abundance is a good indicator of POC quality.

DOC: Our next step was to test whether DOC increased with POC. Most of this DOC is likely derived from larger POC that has been degraded within wetlands and organic soils (47, 49), similar to processes occurring in our lake deltas and ultimately consistent with the landscape to POC to DOC pathway in our trophic upsurge hypothesis. POC is an integrated measure sampled over the entire period of May 22 to June 24, and so we averaged the eight DOC samples collected per site during this time period so their values were comparable. Averaging has the additional benefit of reducing temporal variability in DOC. DOC can vary by several orders of magnitude at our site due to short-lived pulse events that occur over a period of hours and alter the water chemistry of stream outflows (49). At one site, however, we did observe extremely high values of DOC even after averaging across samples; values in the upper quartile ranged from 5.4 – 8.9 versus 2.8 – 3.4 mg L^{-1}at all other sites. The site was located beneath the largest

wetland complex, so rather than remove this outlying observation from our analysis, we accounted for the wetland influence in our model. The influence of wetlands on DOC will also depend on their distance to shoreline because of within-stream degradation of dissolved OM, which becomes increasingly important as wetlands are further from the littoral zone and streams retain water for longer (50, 51). Therefore, we derived a distance-weighted measure of wetland area WA_i by multiplying absolute wetland area in each catchment by the shortest distance from the wetland boundary to lake shoreline (D_i), expressed relative to the shortest distance observed among sites, i.e. $D_i^{-1} / \max_{D>0} D_i^{-1}$. We then modelled mean DOC_i in each site i as a function of $tPOC_i$ and WA_i:

$$DOC_i \sim \ln N(\mu_i^{(2)}, \sigma^{(2)}),$$

$$\mu_i^{(2)} = \alpha_2 + \beta_3 tPOC_i + \beta_4 WA_i, \quad (5)$$

where α_2 is the mean estimated DOC across sites and $\sigma^{(2)}$ is the estimated s.d. We did not include POC quality into Supplementary equation (5), as measured by the ratio of organic to inorganic POC, because it was positively correlated with WA_i, as expected [$r = 0.63$; $p = 0.047$ for one-tailed test; $r > 0.70$ between parameter estimates when included in Supplementary equation (5)].

The benefit of incorporating WA_i is that it also accounts for the fact that wetlands are direct sources of DOC, as organic soils are in contact with surface waters and release large amounts of material during snowmelt and precipitation events (52, 53). This spatial-dependence explains why replacement of WA_i by W_i results in a much less supported model, as measured by the deviance information criterion (DIC; $\Delta DIC = 42$; ref. 54). By contrast, we did not consider the influence of upland forests because their soils often lack a hydrological connection (55), and their vegetation and soils directly produce negligible quantities of DOC (56, 57). For example, root exudation releases only 2 – 4% of photosynthate production and most is rapidly assimilated

by microbes (58). Similarly, POC may be much less sensitive to distance of the wetland from the shoreline because it is derived from more sources than DOC, including riparian vegetation along the length of the discharge stream. POC is also controlled largely by rainfall events, as material must be washed into drainage streams before it is deposited in littoral zones (59), and this occurs irrespective of distance from the lake shoreline. Consequently, replacing W_i in Supplementary equation (4) by WA_i had less supported ($\Delta DIC = 5$).

Bacteria: Our interest was in testing whether bacterial densities increased with DOC concentrations in each site. However, rather than generate a site-level measure of bacterial densities from a single "snap-shot" in the field, we counted the number of bacteria in 9 – 10 water samples per site across different dates and modelled these as a Poisson distributed variable with rate λ_{ij} for each site i on sampling date j. We did not model these data from a normal distribution because this generates continuous-valued expectations and our observations were inherently discrete counts. Our approach then allowed us to deconstruct λ_{ij} into the sum of an estimated site B_i and date B_j component, from which we could relate B_i to the median DOC concentration at each site. We used medians to minimize the leverage associated with flash DOC events that positively skewed means. We also accounted for variation in DOC quality using the mean fluorescence index F_i at each site. Parameter estimates associated with other fluorescence measures, such as the freshness and humification indices (24), were closely correlated with DOC when included in our model ($r > 0.80$), so were not considered here. Two other important considerations of bacterial densities that we accounted for were water temperatures averaged across the period during which bacteria were sampled (T_i) and potential competitive interactions with phytoplankton, measured as the mean of total phytoplankton concentrations in each site (PP_i). Our final model for λ_{ij} was:

$$\ln(\lambda_{ij}) = B_i + B_j,$$

$$B_i = \alpha_3 + \beta_5 \ln(DOC_i) + \beta_6 F_i + \beta_{7i} + \beta_8 T_i + \beta_9 PP_i + \varepsilon_i, \quad (6)$$

where B_j represents random variation among sampling days and is estimated from distribution that is $N(0, \sigma)$, with σ also estimated, α_3 is the mean estimated count across sites and dates for 40 replicates, β_{7i} is the change in the mean for counts derived from only 39 replicates ($n = 3$), and ε_i is the variance in B_i, which is calculated by propagating the error associated with site-level means of DOC_i, F_i, and PP_i.

Zooplankton: We tested whether the biomass of zooplankton (Z_i) trapped in each site *i* increased with bacterial densities. We summed bacterial counts (B_i) across dates within each site *i* to have a measure of potential OM quantity over the period of zooplankton growth at each site, and scaled values where necessary onto a common 40 observations (see above). We also included the quantity of $tPOC_i$, which animals can directly ingest (60, 61). To approximate food quality, we used the ratio of organic to inorganic POC (tPQ_i). We also averaged the summed abundances of Bacillariophyceae, Chlorophyceae, and Cryptophyceae across dates within each site (Q_i). These groups synthesize key fatty acids that supplement high-quality diets for zooplankton (28, 62), as well as provide an autochthonous source of OM to be transferred upwards through the food web. Finally, zooplankton biomass may differ among sites due to predation pressure. We therefore summed the number of planktivorous fish caught within each site across the two dates on which fish communities were gillnetted (PR_i). Most individuals were yellow perch (692 of 736), and we removed those >95 mm in length because they begin to shift their diet at this size towards small fish and pelagic animals at our site (16). We then assumed that Z_i followed a log-normal distribution, with an estimated s.d. $\sigma^{(3)}$ and mean $\mu_i^{(3)}$:

$$\mu_i^{(3)} = \alpha_4 + \beta_{10} B_i + \beta_{11} tPOC_i + \beta_{12} tPQ_i + \beta_{13} Q_i + \beta_{14} PR_i, \quad (7)$$

where α_4 is the mean estimated mass across sites.

YOY Fish: We tested the prediction that the fresh weight of YOY perch (M_i) increased with total amount of zooplankton biomass Z_i in each site *i*. As with bacterial densities, it was not possible to obtain a single perch "weight" at each site. Rather, we measured sizes of individual fish *l* in each site *i* (M_{il}) and decomposed this into the sum of a site-level mean (M_i) plus random variation associated with each individual *l* in that site (υ_{il}). We then related M_i to Z_i, the mean water temperature during the time of fish growth T_i, and the number of perch <100 mm long caught from our gillnet sampling (D_i), to account for effects of density-dependence on growth (63, 64). Growth may also be influenced by risk of predation (16, 65–67). Across both sampling events, we caught only one individual of walleye (*Sander vitreus*), pike (*Esox lucius*) and smallmouth bass (*Micropterus dolomieu*) within gillnets at four of the eight sites, and only 4 – 6 individuals at the other sites. Given the low absolute catch, we coded our data into a binary variable of relatively low (=1 individual) and high (>4 individuals) predator abundance P_i and added this to our model.

We considered the effect of food quality on fish growth as the percentage of fatty acid composition in each site comprised by EPA, DHA, and n-6 FA (FA_i). Given the strong correlations among these three classes of FA ($|r| > 0.87$-0.91), we could not use all of them directly as predictors of M_i. Rather, we used a latent variable approach that assumed M_i was influenced by an unobserved variable representing overall FA composition at each site η_i, which could then be related to each of the three observed FA classes (68). EPA and n-6 FA were modelled from normal distributions, while DHA was modelled from a log-normal, and all had means estimated as linear products of η_i and estimated variances. We did not group EPA and DHA into one category of n-3 FA because they were negatively correlated ($r = -0.91$), reflecting associations with different zooplankton communities (Supplementary Fig. 2). Cladocera preferentially accumulate EPA, while Copepods accumulate DHA (69), and the latter did have

greater mass fractions of DHA in our sites (Supplementary Table 1). This dependency of FA on zooplankton communities also introduced correlation between η_i and zooplankton biomass Z_i. As zooplankton communities became heavier at our site, we found that the ratio of Cladocera to Copepod species increased (r = 0.66), and so the mass fraction of DHA decreased while EPA increased (r = -0.59 and 0.80, respectively). To account for this, we let η_i be equal to FA composition independent of zooplankton biomass ξ_i plus Z_i. We then randomly sampled ξ_i from a normal distribution with mean centered at zero and estimated s.d., and modelled M_{il} as:

$$M_{il} = M_i + \upsilon_{il},$$

$$M_i = \alpha_5 + \beta_{15}Z_i + \beta_{16}T_i + \beta_{17}D_i + \alpha_6 P_i + \beta_{18}\xi_i, \quad (8)$$

where υ_{il} is the variation among individuals in each site and is estimated from a distribution that is ~ $N(0, \sigma_i^{(4)})$, with $\sigma_i^{(4)}$ also estimated, and α_5 and $\alpha_5 + \alpha_6$ are the mean sizes among sites at low and high predation, respectively. We let each FA class be ~ $N(\gamma\eta_i, \sigma)$, with separately estimated γ and σ, $\eta_i = \xi_i + Z_i$, and $\xi_i \sim N(0, \sigma^{(5)})$, with $\sigma^{(5)}$ also estimated. All of EPA, DHA, and n-6 FA were well-predicted by the resulting models, demonstrating that our latent variable was successfully parameterized from observed data (Supplementary Fig. 8).

Statistical analysis of allochthonous support

Our mixing model assumed that the ratios of $\delta^{13}C$, $\delta^{15}N$, and $\delta^{2}H$ in fish i from site j were each drawn from a normal distribution with estimated mean μ_j and s.d. σ_j. Although the observed $\delta^{13}C$ ratios ($C_{\delta C,ij}$) were right-skewed, we accounted for this by assuming values were drawn from a Student's t-distribution. Small samples from symmetric long-tailed distributions, such as the t-distribution, can appear asymmetric without the underlying distribution being skewed, and there was no reason to believe that was the case for $\delta^{13}C$. The t-distribution is ultimately analogous to a normal distribution that has been compounded with heavy tailed variance that is shortened as

the estimated degrees of freedom χ increase. Given this formulation, we assumed that $\mu_{\delta C,j}$ could be described by the relative contributions of the mean terrestrial ($T_{\delta C,j}$), littoral ($L_{\delta C,j}$), and benthic ($B_{\delta C,j}$) sources of $\delta^{13}C$ in each site j:

$$C_{\delta C,ij} \sim St_t(\mu_{\delta C,j}, \psi_{\delta C,j}, \chi),$$

$$\mu_{\delta C,j} = \phi_{T,j}T_{\delta C,j} + \phi_{L,j}L_{\delta C,j} + \phi_{B,j}B_{\delta C,j}. \quad (9)$$

The coefficients $\phi_{T,j}$, $\phi_{L,j}$, and $\phi_{B,j}$ represented the estimated proportional use by fish of terrestrial, littoral (i.e. vertically-migrating zooplankton in the near-shore photic zone), and benthic resources at each site j, respectively. To ensure that the ϕ's summed to one, we inversely transformed parameters from log-ratios centered on geometric means as in Solomon et al. (70). We then propagated the uncertainty into $\sigma_{\delta C,j}$ associated with the observed $\delta^{13}C$ sources $T_{\delta C,j}$, $L_{\delta C,j}$, $B_{\delta C,j}$, which were averaged in each site j. We did so by summing the product of the estimated effects and the observed variances of their respective covariates, and added this to an estimated value of $\varepsilon_{\delta C}$ that was sampled from a normal distribution with mean of zero and estimated s.d. σ_C to generate $\psi_{\delta C,j}$. $\sigma_{\delta C,j}$ scales with $\psi_{\delta C,j}$ and is equal to $[\psi_{\delta C,j}\chi/(\chi - 2)]^{0.5}$.

For estimating the $\delta^{15}N$ ratio ($C_{\delta N,ij}$), we used the same approach as for $\delta^{13}C$ but also considered that $\delta^{15}N$ becomes progressively enriched as trophic levels increase (71). We accounted for this by adding Δ_{tot} to Supplementary equation (9) and estimating $C_{\delta N,ij}$ from a normal distribution as:

$$C_{\delta N,ij} \sim N(\mu_{\delta N,j}, \sigma_{\delta N,j}),$$

$$\mu_{\delta N,j} = \phi_{T,j}T_{\delta N,j} + \phi_{L,j}L_{\delta N,j} + \phi_{B,j}B_{\delta N,j} + \Delta_{tot}. \quad (10)$$

We estimated Δ_{tot} as the product of the estimated per-trophic-level isotopic enrichment of N (Δ_N) and trophic position of YOY perch (τ), defined as trophic levels above primary producers (70):

$$\Delta_{tot} \sim N(\mu_{\Delta tot}, \sigma_{\Delta tot}),$$

$$\mu_{\Delta tot} = \Delta_N \times \tau,$$

where estimates of Δ_N and τ were constrained with data. Δ_N was drawn from a distribution that was ~N(2.52, 1.46), which is based on data from 40 taxa (71), and τ was estimated from a distribution was ~N(2.5, 0.1), based on data for juvenile and YOY fish from Wisconsin (70). We used the estimated values of Δ_N and τ and their observed standard deviations to calculate $\sigma_{\Delta tot}$ as $[(1.46/\Delta_N)^2 + (0.1/\tau)^2]\mu_{\Delta tot}^2$, so $\sigma_{\Delta tot}$ was not directly estimated.

Finally, we estimated δ^2H ratios ($C_{\delta H,ij}$) using Supplementary equation (9), but considered that measured values were influenced by water consumed in the diets of fish (72). We specifically estimated the contribution of dietary water to δ^2H fractionations by measuring the ratio of δ^2H in water at each site ($W_{\delta H,j}$). Water samples were collected on May 28, June 7, and June 18 using protocols described in main text and stored at 4 ºC until analysis on a cavity-ring-down laser spectrometer (73). We then estimated the proportion of δ^2H in YOY perch that was derived solely from environmental water ($\omega_{tot,j}$) as one minus the proportion of δ^2H derived from diet, accounting for the fact that diet, and hence water consumption, will vary among sites by estimating j different values. We also allowed the estimated per-trophic-level contribution of water ω to decline with increasing trophic levels τ above the dietary end members. The littoral end member $L_{\delta H,j}$ occurred at a different trophic level than $T_{\delta H,j}$ and $B_{\delta H,j}$, which were primary producers, so we estimated the trophic position of fish relative to that of zooplankton τ_{zoo} and a third of the total dietary contribution towards δ^2H was attributed to $L_{\delta H,j}$. τ_{zoo} was itself estimated from a distribution was ~N(1.75, 0.2), averaging data for both herbivorous and carnivorous zooplankton from Wisconsin and allowing for a relatively larger s.d. (70). We then estimated $\omega_{tot,j}$ from a Beta distribution, as values varied between 0 and 1, with a mean equal to: $\overline{\omega}_{tot,j} = 1 - \frac{2}{3}(1-\omega)^{\tau} - \frac{1}{3}(1-\omega)^{\tau-\tau_{zoo}}$. The s.d. of the Beta distribution incorporated uncertainty

in ω, τ, τ_{zoo} based on generalized equations for propagating normally-distributed errors (74); see model Supplementary Software 1. ω had a mean of 0.12 and s.d. of 0.02, as used in previous isotopic mixing models for fishes, including yellow perch (72, 75). $C_{\delta H,ij}$ was then expressed as:

$$C_{\delta H,ij} \sim N(\mu_{\delta H,j}, \sigma_{\delta H,j}),$$

$$\mu_{\delta H,j} = \omega_{tot,j} W_{\delta H,j} + (1 - \omega_{tot,j})(\phi_{T,j} T_{\delta H,j} + \phi_{L,j} L_{\delta H,j} + \phi_{B,j} B_{\delta H,j}). \quad (11)$$

Observed variance in $W_{\delta H,j}$ was propagated along with that of $T_{\delta H,j}$, $P_{\delta H,j}$, and $B_{\delta H,j}$ and added to the estimated value of $\varepsilon_{\delta H}$ to calculate $\sigma_{\delta H,j}$.

To test whether allochthonous support of fish changed with land cover, we estimated $\phi_{T,j}$ in our mixing model (Supplementary equations 9–11) as a direct function of the mean NDVI value within each catchment VD_j and catchment area A_j. This allowed us to separate the amount of variation in resource use explained by catchment area versus relative land use (i.e. vegetation density). Small catchments may weakly influence consumer resource use because they always export relatively little organic matter, irrespective of vegetation density, and vice versa. Wetlands are also a source of organic matter and nutrients (48, 76, 77), so the relative cover of wetlands in each catchment WC_j may explain some of the variation in terrestrial resource use observed in fish. Finally, the effect of VD_j across the entire catchment may depend on soil wetness. Soils that are more waterlogged export greater quantities of OM to surface waters during periods of high runoff, and this increases as more soil is covered in vegetation (78). Therefore, in addition to the independent effects of VD_j and WC_j, we expected additional OM to be provided to sites where both variables were large because of this interaction during periods of high runoff (77, 78). WC_j should directly capture soil wetness because the presence of wetlands – by their very definition – indicate both soil types and local topographies that have a greater potential for becoming waterlogged. We then expressed $\phi_{T,j}$ on a logit-scale to constrain values between zero and one:

$$\text{logit}(\phi_{T,j}) = \alpha_T + \beta_{T,1}VD_j + \beta_{T,2}A_j + \beta_{T,3}WC_j + \beta_{T,4}VD_jWC_j + \varepsilon_j, \quad (12)$$

where α_T was the estimated level of terrestrial resource use observed among sites at the mean values of the covariates (i.e. mean $\phi_{T,j}$ on logit-scale) and ε_j was normally-distributed residual error with estimated s.d. σ_ϕ. We did not use NDVI values solely from the riparian area because $\phi_{T,j}$ also depends on dissolved organic matter, which we show increases with a measure of absolute area, i.e. weighted wetland area (see text associated with Supplementary equation 5 for discussion).

Model estimation

Three MCMC chains of at least 42 000 iterations were simulated for each model, with a burn-in period of at least 40 000 runs. We assigned relatively uninformative priors for all regression coefficients (i.e. α's, β's, and γ's) and standard deviations (i.e. σ's), which were ~ $N(0, 100)$ and $U(0, 100)$, respectively. For ϕ_L and ϕ_B coefficients in the three-isotope mixing model (Supplementary equations 9–12), we placed uniform priors on the interval (-3, 5), which are uninformative in the centered log-ratio space into which ϕ's were transformed for estimation (70, 81). The estimated degrees of freedom parameter χ for the $\delta^{13}C$ model also had a uniform prior but on the interval $(2, \infty)$. All covariates were standardized to a mean of zero and s.d. of one so that their estimated coefficients were directly comparable. To infer effects, we calculated posterior means and 95% credible intervals (CIs) for each parameter by drawing a subset of at least 500 simulations.

We used three approaches to verify convergence of our model. First, we visually assessed all chain traces to ensure proper mixing of posterior distributions. Second, we calculated the potential scale reduction factor $\hat{R}$ for each parameter from each subset of simulations. $\hat{R}$

predicts the extent to which a parameter's confidence intervals will be reduced if models are run for an infinite number of simulations. All our values were less than 1.1, which implies that the model has approximately converged and MCMC chains have mixed (82). Finally, we also ensured that the effective number of simulation draws, n_{eff}, a measure of the independence amongst the subset of simulations, always exceeded 100 (82). We summarized overall model fit by calculating a Bayesian R^2 at the level of our focal response variable, analogous to the proportion of variance explained by a model in classical linear regression (83).

Site affinity of fish

We also tested if fish reflected the chemistry of the sites from which they were collected. Many previous studies have used the molar ratios of elements concentrated within otoliths and other hard tissue as environmental tracers of fish movements and habitat affinity (e.g. 84–87). Thus, we calculated Ba:Ca and Sr:Ca ratios in each fish, and tested whether each ratio r_i for fish i from site j increased with the same ratio measured in water w_j. We assumed that r_i was derived from a log-normal distribution with mean μ_i and estimated σ, and fitted the following using JAGS (as described above for the trophic upsurge models):

$$\mu_i = \alpha_7 + \beta_{25}\ln(w_j) + \beta_{26}\ln(f_i) + \beta_{27}\text{WA}_j, \quad (13)$$

where α_7 is the mean ratio, the β's are estimated, w_j is averaged across five water samples taken between May 28 and June 11 in each site, and WA_j is the weighted measure of wetland area described previously and that is included to account for the influence of wetlands on the delivery of metals. We used spring measurements because fish signatures are most sensitive to metal uptake during larval development (88).

Supplementary References

1. Paterson, A.M. *et al*. Long-term changes in phytoplankton composition in seven Canadian Shield lakes in response to multiple anthropogenic stressors. *Can. J. Fish. Aquat. Sci.* **65**, 846–861 (2008).
2. Stevenson, D.K. & Campana, S.E. (eds). Otolith microstructure examination and analysis. *Can. Spec. Publ. Fish. Aquat. Sci.* **117**, 1–130 (1992).
3. Mansueti, A.J. Early development of the yellow perch, *Perca flavescens*. *Chesapeake Science* **5**, 46–66 (1964).
4. Whiteside, M.C, Swindoll, C.M. & Doolittle, W.L. Factors affecting the early life history of yellow perch, *Perca flavescens*. *Environ. Biol. Fish.* **12**, 47–56 (1985).
5. Fitzgerald, D.G., Dale, A.R., Thomas, M.V. & Sale, P.F. Application of otolith analyses to investigate broad size distributions of young yellow perch in temperate lakes. *J. Fish Biol.* **58**, 248–263 (2001).
6. Huff, D.D., Grad, G. & Williamson, C.E. Environmental constraints on spawning depth of yellow perch: the roles of low temperature and high solar ultraviolet radiation. *Trans. Am. Fish. Soc.* **133**, 718–726 (2004).
7. Bertolo, A. *et al*. Inferring processes from spatial patterns: the role of directional and non–directional forces in shaping fish larvae distribution in a freshwater lake system. PLoS ONE **7**, e50239. (2012).
8. Isermann, D.A & Willis, D.W. Emergence of larval yellow perch (*Perca flavescens*) in South Dakota lakes: potential implications for recruitment. *Fisheries Manage. Ecol.* **15**, 259–271 (2008).

9. Silliman, R.P. Comparison between Gompertz and von Bertalanffy curves for expressing growth in weight of fishes. *Journal of the Fisheries Research Board of Canada* **23**, 15–20 (1966).
10. Ricker W.E. Growth rates and models. *Fish Physiol*. **8**, 677–743 (1979).
11. Katsanevakis, S. & Maravelias, C.D. Modelling fish growth: multi-model inference as a better alternative to a priori using von Bertalanffy equation. *Fish and Fisheries* **9**, 178–187 (2008).
12. Dumas, A., France, J. & Bureau, D. Modelling growth and body composition in fish nutrition: where have we been and where are we going? *Aquac. Res*. **41**, 161–181 (2010).
13. Essington, T.E., Kitchell, J.F. & Walters, C. The von Bertalanffy growth function, bioenergetics, and the consumption rates of fish. *Can. J. Fish. Aquat. Sci*. **58**, 2129–2138 (2001).
14. West, G.N., Brown, J.H. & Enquist, B.J. A general model for ontogenetic growth. *Nature* **413**, 628–631 (2001).
15. Chen, Y., Jackson, D.A. & Harvey, H.H. A comparison of von Bertalanffy and polynomial functions in modelling fish growth data *Can. J. Fish. Aquat. Sci*. **49**, 1228–1235 (1992).
16. Lippert, K.A., Gunn, J.M. & Morgan, G.E. Effects of colonizing predators on yellow perch (*Perca flavescens*) populations in lakes recovering from acidification and metal stress. *Can. J. Fish. Aquat. Sci.* **64**, 1413–1428 (2007).
17. National Aeronautics and Space Administration [NASA] *Landsat 7 Science Data Users Handbook* (NASA, Washington, D.C., 2011).
18. Tucker, C.J. & Sellers, P.J. Satellite remote sensing of primary production. *International Journal of Remote Sensing* **7**, 1395–1416 (1986).

19. Pettorelli, N. *et al*. Using the satellite-derived NDVI to assess ecological responses to environmental change. *Trends Ecol*. *Evol*. **20**, 503–510 (2005).
20. Tanre, D., Holben, B.N. & Kaufman, Y.J. Atmospheric correction against algorithm for NOAA-AVHRR products: theory and application. *IEEE Trans*. *Geosci*. *Remote Sens*. **30**, 231–248 (1992).
21. Ontario Ministry of Natural Resources [OMNR] *Forest Resource Inventory Digital Aerial Imagery* (OMNR, Peterborough, 2009).
22. Szkokan-Emilson, E.J., Wesolek, B.E. & Gunn, J.M. Terrestrial organic matter as subsidies that aid in the recovery of macroinvertebrates in industrially damaged lakes. *Ecol*. *App*. **21**, 2082–2093 (2011).
23. Cory, R.M. & McKnight, D.M. Fluorescence spectroscopy reveals ubiquitous presence of oxidized and reduced quinones in DOM. *Environ*. *Sci*. *Technol*. **39**, 8142–8149 (2005).
24. Fellman, J.B., Hood, E. & Spencer, R.G.M. Fluorescence spectroscopy opens new windows into dissolved organic matter dynamics in freshwater ecosystems: a review. *Limnol. Oceanogr*. **55**, 2452–2462 (2010).
25. Zelles, L. Fatty acid patterns of phospholipids and lipopolysaccharides in the characterisation of microbial communities in soil: a review. *Biol*. *Fertil*. *Soils* **29**, 111–129 (1999).
26. Sargent, J., Bell, G., McEvoy, L., Tocher, D. & Estevez, A. Recent developments in the essential fatty acid nutrition of fish. *Aquaculture* **177**, 191–199 (1999).
27. Brett, M. & Müller-Navarra, D. The role of highly unsaturated fatty acids in aquatic foodweb processes. *Freshw. Biol.* **38**, 483–499 (1997).
28. Brett, M.T., Kainz, M.J., Taipale, S.J. & Seshan, H. Phytoplankton, not allochthonous carbon, sustains herbivorous zooplankton production. *Proc. Natl. Acad. Sci. USA* **106**, 21197–21201 (2009).

29. McMeans, B.C., Arts, M.T., Rush, S.A. & Fisk, A.T. Seasonal patterns in fatty acids of *Calanus hyperboreus* (Copepoda, Calanoida) from Cumberland Sound, Baffin Island, Nunavut. *Mar. Biol.* **159**, 1095–1105 (2012).
30. Tocher, D.R. Metabolism and functions of lipids and fatty acids in teleost Fish. *Reviews in Fisheries Science* **11**, 107–184 (2003).
31. Smith D.M. *et al*. Essential fatty acids in the diet of silver perch (*Bidyanus bidyanus*): effect of linolenic and linoleic acid on growth and survival. *Aquaculture* **236**, 377–390 (2004).
32. Brown, P.B., Dabrowski, K. & Garling, D.L. Nutrition and feeding of yellow perch (*Perca flavescens*) *J. Appl. Ichthyol.* **12**, 171–174 (1996).
33. Castell, J.D., Bell, J.G., Tocher, D.R. & Sargent, J.R. Effects of purified diets containing different combinations of arachidonic and docosahexaenoic acid on survival, growth and fatty acid composition of juvenile turbot (*Scophthalmus maximus*). *Aquaculture* **128**, 315–333 (1994).
34. Kainz, M., Arts, M.T. & Mazumder, A. Essential fatty acids in the planktonic food web and their ecological role for higher trophic levels. *Limnol. Oceanogr.* **49**, 1784–1793 (2004).
35. Czesny, S.J. *et al*. Fatty acid signatures of Lake Michigan prey fish and invertebrates: among-species differences and spatiotemporal variability. *Can. J. Fish. Aquat. Sci.* **68**, 1211–1230 (2011).
36. Ballantyne, A.P., Brett, M.T. & Schindler, D.E. The importance of dietary phosphorus and highly unsaturated fatty acids for sockeye (*Oncorhynchus nerka*) growth in Lake Washington a bioenergetics approach. *Can. J. Fish. Aquat. Sci.* **60**, 12–22 (2003).
37. Arts, M.T. & Kohler, C.C. Health and condition in fish: the influence of lipids on membrane competency and immune response. *Lipids in Aquatic Ecosystems* Kainz, M., Brett, M.T. & Arts, M.T. (eds) 237–256 (Springer, New York, 2009).

38. Rosauer, D.R. *et al*. Development of yellow perch (*Perca flavescens*) broodstocks: Initial characterization of growth and quality traits following grow-out of different stocks. *Aquaculture* **317**, 58–66 (2011).
39. del Giorgio, P.A. & Cole, J.J. Bacterial growth efficiency in natural aquatic ecosystems. *Annu. Rev. Ecol. Syst.* **29**, 503–541 (1998).
40. Vrede, K. Nutrient and temperature limitation of bacterioplankton growth in temperate lakes. *Microb. Ecol.* **49**, 245–256 (2005).
41. Hall, E.K. & Cotner, J.B. Interactive effect of temperature and resources on carbon cycling by freshwater bacterioplankton communities. *Aquat. Microb. Ecol.* **49**, 35–45 (2007).
42. George, D.G. & Harris, G.P. The effect of climate on long-term changes in the crustacean zooplankton biomass of Lake Windermere, UK. *Nature* **316**, 536–539 (1985).
43. Coble, D.W. Dependence of total annual growth in yellow perch on temperature. *Journal of the Fisheries Research Board of Canada* **23**, 15–20 (1966).
44. Power, M. & van den Heuvel, M.R. Age-0 yellow perch growth and its relationship to temperature. *Trans. Am. Fish. Soc.* **128**, 687–700 (1999).
45. Appelberg, M. Swedish standard methods for sampling freshwater fish with multi-mesh gillnets. *Fiskeriverket Information* **1**, 3–32 (2000).
46. Wetzel, R.G. *Limnology: Lake and River Ecosystems* (Academic Press, San Diego, 2001).
47. Wickland, K.P., Neff, J.C. & Aiken, G.R. Dissolved organic carbon in Alaskan boreal forest: sources, chemical characteristics, and biodegradability. *Ecosystems* **10**, 1323–1340 (2007).
48. Dillon, P.J. & Molot, L.A. Effect of landscape form on export of dissolved organic carbon, iron, and phosphorus from forested stream catchments. *Water Resour. Res.* **33**, 2591–2600 (1997).

49. Szkokan-Emilson, E.J., Watmough, S., Gunn, J.M. & Kielstra, B. Drought-induced release of metals from peatlands in watersheds recovering from historical metal and sulphur deposition. *Biogeochemistry* **116**, 131–145 (2013).
50. Gergel, S.E., Turner, M.G. & Kratz, T.K. Dissolved organic carbon as an indicator of the scale of watershed influence on lakes and rivers. *Ecol. App*. **9**, 1377–1390 (1999).
51. Canham, C.D. *et al*. A spatially explicit watershed-scale analysis of dissolved organic carbon in Adirondack lakes. *Ecol*. *App*. **14**, 839–854 (2004).
52. Schiff, S. *et al*. Precambrian Shield wetlands: hydrologic control of the sources and export of dissolved organic matter. *Clim. Change* **40**, 167–188 (1998).
53. Burns, D. What do hydrologists mean when they use the term flushing? *Hydrol. Process*. **19**, 1325–1327 (2005).
54. Spiegelhalter, D.J., Best, N.G., Carlin, B.P. & van der Linde, A. Bayesian measures of model complexity and fit. *J. Roy. Stat. Soc. Series B* **64**, 583–639 (2002).
55. Pacific, V.J., Jencso, K.G. & McGlynn, B.L. Variable flushing mechanisms and landscape structure control stream DOC export during snowmelt in a set of nested catchments. *Biogeochemistry* **99**, 193–211 (2010).
56. Kalbitz, K., Solinger S., Park, J.-H., Michalzik, B. & Matzner, E. Controls on the dynamics of dissolved organic matter in soils: a review. *Soil Sci*. **165**, 277–304 (2000).
57. Neff, J.C. & Asner, G.P. Dissolved organic carbon in terrestrial ecosystems: synthesis and a model. *Ecosystems* **4**, 29–48 (2001).
58. Jones, D.L., Hodge, A. & Kuzyakov, Y. Plant and mycorrhizal regulation of rhizodeposition. *New Phytol*. **163**, 459–480 (2004).
59. Golladay, S.W. Suspended particulate organic matter concentration and export in streams. *J. North Am. Benthol. Soc*. **16**:122–131 (1997).

60. Cole, J.J. *et al*. Differential support of lake food webs by three types of terrestrial organic carbon. *Ecol. Lett.* **9**, 558–568 (2006).
61. Bartels, P. *et al*. Terrestrial subsidies to lake food webs: an experimental approach. *Oecologia* **168**, 807–818 (2011).
62. De Lange, H.J. & Arts, M.T. Seston composition and the potential for *Daphnia* growth. *Aquat Ecol* **33**, 387–398 (1999).
63. Henderson, B.A. Factors affecting growth and recruitment of yellow perch, *Perca flavescens* Mitchill, in South Bay, Lake Huron. *J. Fish Biol*. **26**, 449–458 (1985).
64. Post, J.R. & McQueen, D.J. Variability in first-year growth of yellow perch (*Perca flavescens*): predictions from a simple model, observations, and an experiment. *Can. J. Fish. Aquat. Sci.* **51**, 2501–2512 (1994).
65. Post, J.R. & Prankevicius, A.B. Size-selective mortality in young-of-the-year yellow perch (*Perca flavescens*): evidence from otolith microstructure. *Can. J. Fish. Aquat. Sci.* **44**, 1840–1847 (1987).
66. Post, J.R. & Evans, D.O. Size-dependent overwinter mortality of young-of-the-year yellow perch (*Perca flavescens*): laboratory, in situ enclosure, and field experiments. *Can. J. Fish. Aquat. Sci.* **46**, 1958–1968 (1989).
67. Olson, M.H., Green, D.M. & Rudstam, L.G. Changes in yellow perch (*Perca flavescens*) growth associated with the establishment of a walleye (*Stizostedion vitreum*) population in Canadarago Lake, New York (USA). *Ecol. Freshw. Fish* **10**, 11–20 (2001).
68. Shipley, B. *Cause and Correlation in Biology: A User's Guide to Path Analysis, Structural Equations and Causal Inference* (Cambridge University Press, Cambridge, 2000).
69. Ravet, J.L., Brett, M.T. & Arhonditsis, G.B. The effects of seston lipids on zooplankton fatty acid composition in Lake Washington, Washington, USA. *Ecology* **91**, 180–190 (2010)

70. Solomon, C.T. *et al*. Terrestrial, benthic, and pelagic resource use in lakes: results from a three-isotope Bayesian mixing model. *Ecology* **92**, 1115–1125 (2011).
71. Vanderklift, M.A. & Ponsard, S. Sources of variation in consumer-diet δ15N enrichment: a meta-analysis. *Oecologia* **136**, 169–182 (2003).
72. Solomon, C.T. *et al*. The influence of environmental water on the hydrogen stable isotope ratio in aquatic consumers. *Oecologia* **161**, 313–324 (2009).
73. Doucett, R.R., Marks, J.C., Blinn, D.W., Caron, M. & Hungate, B.A. Measuring terrestrial subsidies to aquatic food webs using stable isotopes of hydrogen. *Ecology* **88**, 1587–1592 (2007).
74. Taylor, J.R. *An Introduction to Error Analysis: The Study of Uncertainties in Physical Measurements* (University Science Books, Sausalito, 1997).
75. Batt, R.D. *et al*. Resources supporting the food web of a naturally productive lake. *Limnol. Oceanogr.* **57**, 1443–1452 (2012).
76. Xenopoulos, M.A., Lodge, D.M., Frentress, J., Kreps, T.A., Bridgham, S.D., Grossman, E. & Jackson, C.J. Regional comparisons of watershed determinants of dissolved organic carbon in temperate lakes from the Upper Great Lakes region and selected regions globally. *Limnol. Oceanogr*. **48**, 2321–2334 (2003).
77. Creed, I.F., Beall, F.D., Clair, T.A., Dillon, P.J. & Hesslein, R.H. Predicting export of dissolved organic carbon from forested catchments in glaciated landscapes with shallow soils. *Global Biogeochem. Cy*. **22**, GB4024 (2008).
78. D'Arcy, P. & Carignan R. Influence of catchment topography on water chemistry in southeastern Québec Shield lakes. *Can. J. Fish. Aquat. Sci.* **54**, 2215–2227 (1997).
79. Plummer, M. JAGS: a program for analysis of Bayesian graphical models using Gibbs sampling. *Proceedings of the 3rd International Workshop on Distributed Statistical*

Computing Hornik, K., Leisch, F. & Zeileis, A. (eds) (Technische Universitat Wien, Vienna, 2003).

80. R Development Core Team. *R: A Language and Environment for Statistical Computing* (R Foundation for Statistical Computing, Vienna, 2012).
81. Semmens, B.X., Ward, E.J., Moore, J.W. & Darimont, C.T. Quantifying inter- and intra-population niche variability using hierarchical Bayesian stable isotope mixing models. *PLoS ONE* **4**, e6187 (2009).
82. Gelman, A. & Hill, J. *Data Analysis Using Regression And Multilevel/Hierarchical Models* (Cambridge University Press, Cambridge, 2007).
83. Gelman, A. & Pardoe, I. Bayesian measures of explained variance and pooling in multilevel (hierarchical) models. *Technometrics* **48**, 241–251 (2006).
84. Campana, S.E. & Thorrold, S.R. Otoliths, increments, and elements: keys to a comprehensive understanding of fish populations? *Can. J. Fish. Aquat. Sci.* **58**, 30–38 (2001).
85. Wells, B.K., Rieman, B.E., Clayton, J.L., Horan, D.L. & Jones, C.M. Relationships between water, otolith, and scale chemistries of westslope cutthroat trout from the Coeur d'Alene River, Idaho: the potential application of hard-part chemistry to describe movements in freshwater. *Trans. Am. Fish. Soc.* **132**, 409–424 (2003).
86. Gibson-Reinemer, D.K. *et al*. Elemental signatures in otoliths of hatchery rainbow trout (*Oncorhynchus mykiss*): distinctiveness and utility for detecting origins and movement. *Can. J. Fish. Aquat. Sci.* **66**, 513–524 (2009).
87. Pangle, K.L., Ludsin, S.A. & Fryer, B.J. Otolith microchemistry as a stock identification tool for freshwater fishes: testing its limits in Lake Erie. *Can. J. Fish. Aquat. Sci.* **67**, 1475–1489 (2010).

88. Jezierska, B., Ługowska, K. & Witeska, M. The effects of heavy metals on embryonic development of fish (a review). *Fish Physiol. Biochem.* **35**, 625–640 (2009).